


A process-based decomposition of decadal-scale surface temperature evolutions over East Asia

Junwen Chen^{1,2}  · Yi Deng² · Wenshi Lin¹ · Song Yang¹

Received: 15 February 2017 / Accepted: 18 August 2017 / Published online: 31 August 2017
© Springer-Verlag GmbH Germany 2017

Abstract This study partitions the observed decadal evolution of surface temperature and surface temperature differences between two decades (early 2000s and early 1980s) over the East Asian continent into components associated with individual radiative and non-radiative (dynamical) processes in the context of the coupled atmosphere-surface climate feedback-response analysis method (CFRAM). Rapid warming in this region occurred in late 1980s and early 2000s with a transient pause of warming between the two periods. The rising CO₂ concentration provides a sustained, region-wide warming contribution and surface albedo effect, largely related to snow cover change, is important for warming/cooling over high-latitude and high-elevation regions. Sensible heat flux and surface dynamics dominates the evolution of surface temperature, with latent heat flux and atmospheric dynamics working against them mostly through large-scale and convective/turbulent heat transport. Cloud via its shortwave effect provides positive contributions to

warming over southern Siberia and South China. The long-wave effect associated with water vapor change contributes significant warming over northern India, Tibetan Plateau, and central Siberia. Impacts of solar irradiance and ozone changes are relatively small. The strongest year-to-year temperature fluctuation occurred at a rapid warming (1987–1988) and a rapid cooling (1995–1996) period. The pattern of the rapid warming receives major positive contributions from sensible heat flux with changes in atmospheric dynamics, water vapor, clouds, and albedo providing secondary positive contributions, while surface dynamics and latent heat flux providing negative contributions. The signs of the contributions from individual processes to the rapid cooling are almost opposite to those to the rapid warming.

Keywords Decadal variation · CFRAM · Surface temperature · Radiative process · Dynamical process · East Asia

This paper is a contribution to the special issue on East Asian Climate under Global Warming: Understanding and Projection, consisting of papers from the East Asian Climate (EAC) community and the 13th EAC International Workshop in Beijing, China on 24–25 March 2016, and coordinated by Jianping Li, Huang-Hsiung Hsu, Wei-Chyung Wang, Kyung-Ja Ha, Tim Li, and Akio Kitoh.

✉ Junwen Chen
chjunw@mail2.sysu.edu.cn

✉ Wenshi Lin
linwenshi@mail.sysu.edu.cn

¹ School of Atmospheric Sciences, Sun Yat-sen University, 135 West Xingang Road, Guangzhou 510275, Guangdong, China

² School of Earth and Atmospheric Sciences, Georgia Institute of Technology, Atlanta, GA 30332, USA

1 Introduction

East Asia is a region vulnerable to climate fluctuations with a high population density and rapid economic growth. Governments, as well as the general public, need detailed information to assess the risks and implement mitigation and adaptation strategies in relation to the projected natural and anthropogenic climate changes (IPCC 2013). Research on causes behind global and regional surface temperature variations provide insights into one of the meteorological variables that is most relevant to human comfort and health, especially in boreal summer and winter.

Eurasia has experienced significant climate change during the last few decades, including pronounced winter warming, snow cover decrease, permafrost thawing and surface

air temperature rise (Romanovsky et al. 2010; Serreze et al. 2000; Yang et al. 2002; Ye et al. 2015). The annual, seasonal, and diurnal variability of near-surface temperature and humidity in China has been investigated and results showed that both temperature and humidity increased in late-twentieth-century with larger trends in winter and nighttime (Wang and Gaffen 2001; Hu et al. 2003). Liu et al. (2004) reported an accelerated warming after 1990 in China, while both the daily maximum and minimum surface air temperatures are increasing faster than those for the Northern Hemisphere and the daily temperature range decreased rapidly from 1960 to 1990. Some studies have been seeking the factors related to the surface air temperature change. According to Duan and Xiao (2015), a rapid warming trend over the Tibetan Plateau during 1998–2013, to some degree, might be attributed to cloud-radiation feedback. Yang and Ren (2017) found out that the diurnal surface temperature range has become significantly smaller over Tibetan Plateau but larger in southeastern China during the 1980s–2000s, and the changes in low-level cloud cover and water vapor were main contributors. As well known, East Asia is a major source of aerosols including dust, sulfates, nitrates, black carbon, and organic carbon (Kaufman et al. 2002), and they have net cooling effect on surface through modulating cloud physics and solar radiation in model experiments (Chen et al. 2016; Chung et al. 2010; Li et al. 2011, 2016; Ramanathan and Carmichael 2008; Rosenfeld et al. 2014; Seinfeld et al. 2004). Related to aerosols effect, a significant decreasing trend in total cloud cover and a slightly increasing trend in low cloud cover along with shortened sunshine duration were observed across China from 1950s to 2000s (Liu et al. 2004; Xia 2010a, b). Besides, broad land-use changes due to natural processes and human activities (e.g. urbanization, deforestation, and desertification) might exacerbate surface warming through changing surface sensible/latent heat flux and net radiation (Feng et al. 2012; Park and Sohn 2010; Ren et al. 2008; Saha et al. 2014; Sun et al. 2016; Wang et al. 2013; Yang et al. 2011).

Despite the substantial efforts devoted to understand the surface temperature change, we still need in the literature a systematic examination of regional-scale surface temperature evolution in observation over East Asia. We provide quantitative attribution of radiative and non-radiative (dynamical) processes to the decadal surface temperature evolutions over the East Asian continent. A process-based decomposition of surface temperature differences between two decades (early 2000s and early 1980s) is examined. Furthermore, the decomposition of extreme year-to-year temperature fluctuations enhances our understanding of the differences and similarities of major physical processes involved across the rapid warming and cooling periods. Here we adopt the coupled atmosphere-surface climate feedback-response analysis method (CFRAM, Cai and Lu 2009; Lu

and Cai 2009) to quantify the relative contribution of multiple physical and dynamical processes to surface temperature evolutions in the observation. Most recently, the CFRAM provided a new angle on the formation of global surface and atmospheric temperature anomalies associated with global warming, inter-annual and sub-seasonal variability (e.g. El Niño Southern Oscillation and Northern Annular Mode) and the nature of surface temperature bias in climate model (Chen et al. 2017; Deng et al. 2012, 2013; Hu et al. 2016, 2017; Liu and Zhou 2017; Liu et al. 2015; Park et al. 2012, 2013; Ren et al. 2016; Yang et al. 2015). Following this introduction, Sect. 2 provides a brief description of the CFRAM method and the observational data. The main results are reported and discussed in Sect. 3. Section 4 gives concluding remarks.

2 Data and method

The observation data used is the European Centre for Medium-range Weather Forecasts (ECMWF) Re-Analysis Interim (ERA-Interim; Dee et al. 2011). ERA-Interim is the latest ECMWF global atmospheric reanalysis covering the period 1979 to present and has a 0.75° horizontal resolution with 37 pressure levels in the vertical ranging from 1000 to 1 hPa. ERA-Interim has been proven to be a good proxy for the in situ surface observation over central Asia (Hu et al. 2014) and the biases over the Tibetan Plateau were smaller than other reanalysis datasets (Bao and Zhang 2013; Wang and Zeng 2012).

The basis of CFRAM is the total energy balance within an atmosphere-surface column consisting of M atmospheric layers and one surface layer (Cai and Lu 2009; Lu and Cai 2009). Writing the total energy balance equation separately for two climate states (climate “A” and “B”), then taking the difference Δ between the two (i.e., “B” minus “A”), we obtain

$$\Delta \frac{\partial E}{\partial t} = \Delta S - \Delta R + \Delta Q^{non-radiative}, \quad (1)$$

where S (R) is the vertical profile of the convergence (divergence) of shortwave (longwave) radiation flux and E is the vertical profile of the total energy for the atmosphere-surface column including latent heat, dry static energy and kinetic energy. For the surface layer of the column, $Q^{non-radiative}$ represents the net convergence of energy due to oceanic motions of all scales over the ocean surfaces while $Q^{non-radiative}$ corresponds to the energy convergence in the column due to runoff, soil heat diffusion, snow/ice freezing and melting over the land/snow/ice surfaces. For the atmospheric layers in the column, $Q^{non-radiative}$ represents the vertical profile of the total energy convergence due to convective, turbulent, and large-scale atmospheric motions. $\frac{\partial E}{\partial t}$ represents the rate of energy and heat storage change, which is substantial in

the ocean but can be neglected in the atmosphere under the condition that annual mean states are considered. All terms in Eq. (1) have units of watts per meter square (W/m²).

By neglecting the interactions among different radiative species and linearizing the radiative energy perturbations, we may express ΔS and ΔR as the sum of partial radiative energy flux convergence/divergence due to individual radiative processes:

$$\begin{aligned} \Delta S &\approx \Delta S^{(SR)} + \Delta S^{(CLD)} + \Delta S^{(WV)} + \Delta S^{(O_3)} + \Delta S^{(AL)} \text{ and} \\ \Delta R &\approx \Delta R^{(CO_2)} + \Delta R^{(CLD)} + \Delta R^{(WV)} + \Delta R^{(O_3)} + \frac{\partial R}{\partial T} \Delta T. \end{aligned} \tag{2}$$

In Eq. (2), abbreviation *SR*, *CLD*, *WV*, *O₃*, *AL*, and *CO₂*, stand for solar irradiance, cloud, water vapor, ozone, surface albedo, and CO₂, respectively. Elements of ΔT are the temperature differences in each layer between two climate states, and $\frac{\partial R}{\partial T}$ is the Planck feedback matrix measuring the vertical profile change of longwave radiation flux divergence due to changes in surface and atmospheric temperatures. By substituting Eq. (2) into Eq. (1), rearranging the terms and multiplying both sides by $(\frac{\partial R}{\partial T})^{-1}$, we obtain

$$\begin{aligned} \Delta T = \left(\frac{\partial R}{\partial T}\right)^{-1} &\left[\Delta S^{(SR)} - \Delta R^{(CO_2)} + \Delta(S - R)^{(CLD)} \right. \\ &+ \Delta(S - R)^{(WV)} + \Delta(S - R)^{(O_3)} + \Delta S^{(AL)} \\ &\left. + \Delta Q^{(SH)} + \Delta Q^{(LH)} + \Delta Q^{(atmos_dyn)} + \Delta Q^{(surf_dyn)} \right], \end{aligned} \tag{3}$$

where $\Delta Q^{(SH)}$ and $\Delta Q^{(LH)}$ are energy differences due to changes in surface turbulent sensible and latent heat fluxes, respectively. $\Delta Q^{(atmos_dyn)} = \Delta Q^{non-radiative}$ in the atmospheric layers, which is estimated as a residual from the radiative energy perturbations in the actual calculations, i.e., $\Delta Q^{(atmos_dyn)} = -\Delta(S - R)^{(atmosphere)}$ and $\Delta Q^{(atmos_dyn)}$ is zero at the surface layer. Similarly, $\Delta Q^{(surf_dyn)}$ is zero in the atmospheric layers and $\Delta Q^{(surf_dyn)} = -\Delta \frac{\partial E}{\partial t} + \Delta Q^{non-radiative} = -\Delta(S - R)^{(surface)} + \Delta Q^{(LH)} + \Delta Q^{(SH)}$ at the surface layer. Equation (3) enable us to express the vertical profile of the temperature differences between two climate states at a given location as the sum of the vertical profile of partial temperature differences due to (from left to right) changes in solar irradiance, CO₂, cloud, water vapor, ozone, surface albedo, surface sensible heat flux, surface latent heat flux, atmospheric dynamics (i.e., energy transport by all scales atmospheric motions), and surface dynamics. Note that the surface (including all substances underneath) is treated as single layer in the context of CFRAM, thus surface dynamics include energy gain/loss due to snow/ice freezing and melting, runoff transport and soil heat diffusion over the land grid points. We adopt the Fu-Liou radiative transfer model (Fu and Liou 1992, 1993) in the evaluation of the individual radiative energy

perturbations in Eq. (3), for example $\Delta(S - R)^{(WV)}$, by conducting “off-line” radiative transfer calculations separately for climate state “A” (“base state”) and a perturbed state where all the atmospheric/surface properties are kept the same as in climate state “A” except that water vapor properties are replaced with those in climate state “B”. The net radiative heating difference between the perturbed state and the base state provides us $\Delta(S - R)^{(WV)}$, i.e., radiative heating difference due to changes in water vapor alone. The Planck feedback matrix is evaluated through documenting the changes in the vertical profile of the longwave radiative heating due to 1 K warming (with respect to the base state temperature) at an atmospheric or a surface layer by conducting multiple radiative transfer calculations. Finally, we need extra caution on the interpretation of surface dynamics and atmospheric dynamics terms, given the way both terms are estimated as residuals from the equation of surface or atmospheric energy balance in the context of CFRAM calculation. They by definition incorporate errors associated with offline radiative transfer calculations and linearization done in the CFRAM. However, dynamical energy transports and energy gain/loss due to surface and soil processes tend to dominate these two terms. In addition, processes not included in current CFRAM analysis also contribute to these two terms, which could be significant at local and regional scales. For example, effects of greenhouse gases (e.g., CH₄, N₂O) and aerosols that are not explicitly considered in the CFRAM are included in atmospheric dynamics.

Variables required as input to the off-line radiative transfer model, including air/surface temperatures, specific humidity, cloud amount, cloud liquid/ice water mixing ratio, solar irradiance at the top of the atmosphere (TOA), CO₂ mixing ratio, ozone mixing ratio, surface albedo, and surface latent/sensible heat flux, are obtained from ERA-Interim. Except for the solar irradiance and CO₂ mixing ratio, we used values from the historical time-dependent external forcings (Taylor et al. 2012). Here we consider the mean state of 1981–1985 (denoted as year “1983” hereafter) as the base state, and following segments (with 1 year increment a time) of 5-year mean state as the climate state to contrast with the base state. That is to say, 1981–1985 is the base state (climate state “A” as discussed before) with multiple climate state “B”’s starting from 1982 to 86 (denoted as year “1984” hereafter), 1983–1987 (“1985”) ... until 2001–2005 (“2003”). For each climate state, composite of 3D and 2D fields used in radiative transfer calculations are constructed with the ERA-Interim data. The CFRAM analysis thus provides temporospatial evolutions of the atmospheric and surface temperature associated with individual physical and dynamical processes through the period of 1981–2005.

3 Results

3.1 Temporospatial structure of the process-based surface temperature attributions

We use the partial temperature differences derived from CFRAM calculations to study the relative contributions of the physical and dynamical processes to the decadal evolutions of observed surface temperature from 1981 to 2005 over the East Asian continent. Figure 1a shows the temporal evolution of area averaged (15° – 70° N, 70° – 160° E, land only) surface temperature (as departures from the average of the base state (1981–1985)) and Fig. 1b–k are the partial temperature associated with changes in solar irradiance, ozone, CO₂, water vapor, surface albedo, clouds, surface dynamics, surface sensible heat flux, surface latent heat flux, and atmospheric dynamics. The temporal evolutions of total partial temperature differences derived from the CFRAM (Fig. 1a, solid line) matched well with the observed surface temperature evolutions in the ERA-Interim (Fig. 1a, dashed line), suggesting that the CFRAM are reasonable approximations to make in this analysis. Obviously, rapid warming occurred in the late 1980s and the early 2000s with a transient pause of warming during the 1990s (Fig. 1a). The overall warming trend is largely driven by changes in CO₂ (Fig. 1d), water vapor (Fig. 1e), clouds (Fig. 1g), surface dynamics (Fig. 1h, mainly energy processes related to snow/ice melting/freezing, river runoff, and soil heat diffusion), and sensible heat flux (Fig. 1i). CO₂ maintains positive contributions to the warming trend through the whole period while contributions from other processes have large interannual variations. Sensible heat flux acts as the main contributor to the warming followed by surface dynamics and clouds, with a time-mean partial temperature difference of approximately 0.42, 0.34 and 0.19 K respectively (upper right corners of Fig. 1i, h, g), while the latent heat flux and atmospheric dynamics play as the main negative contributors to the warming (–0.66 and –0.43 K, Fig. 1j, k). Note that cloud fields in the ERA-Interim have substantial uncertainties related to the microphysics and cumulus parameterizations of the model. The partial temperature results suggest significant positive contributions to the rapid warming in late 1980s from the changes in sensible heat flux (Fig. 1i), water vapor (Fig. 1e) and atmospheric dynamics (Fig. 1k), while latent heat flux tends to work against them (Fig. 1j). The transient pause of warming in the 1990s with several interannual fluctuations mostly originated from the changes in clouds, sensible heat flux, and latent heat flux and the balances of energy perturbations due to changes in water vapor, surface dynamics, and atmospheric dynamics. The atmospheric dynamics gives sustained strong positive contribution to the surface cooling occurred in early 1990s containing some degree of the effect related to the Pinatubo

eruption (Meehl and Teng 2012). The recovery of warming in early 2000s mainly comes from the changes in clouds, surface dynamics, and atmospheric dynamics, weakened by water vapor and surface albedo effects. The positive effect of surface albedo decreased dramatically after 1999 and eventually became negative (Fig. 1f). In order to better understand this change, we examine the surface albedo differences and snowfall differences between 2003 (5-year mean of 2001–2005) and 1999 (1997–2001) using the ERA-Interim data (Fig. 2). Results show that the sharp negative contribution from surface albedo after 1999 is connected to the more than 1% increasing of the surface albedo over northern Siberia, Mongolia, and the Tibetan Plateau from 1999 to 2003 as shown in Fig. 2a, reflecting more solar radiation back to the atmosphere, which is consistent with previous studies (e.g. Jeong et al. 2011). Furthermore, the surface albedo change is closely related to the increased snowfall over those areas (Fig. 2a v.s. b), and the pattern correlation coefficient between them is 0.36. The effect of solar irradiance (Fig. 1b), largely associated with the quasi 11-years solar cycle, and the effect of ozone (Fig. 1c) are much weaker on the surface temperature evolutions compared to the effects of other processes during this period.

The various physical processes contributing to the surface warming from early 1980s to early 2000s are investigated. The surface temperature differences between 2003 (2001–2005) and base state (1981–1985) over the East Asian continent is shown in Fig. 3a, and the partial temperature differences associated with individual radiative and non-radiative processes are displayed in Fig. 3b–k. The most pronounced feature in Fig. 3a is the strong warming over southern Siberia and East China. The rising CO₂ concentration in the atmosphere gives nearly uniform warming with an area averaged partial temperature difference of approximately 0.17 K (upper right corners of Fig. 3d). Solar forcing provides a net warming effect but it's one magnitude smaller compared to the CO₂ effect (Fig. 3b v.s. Fig. 3d). The ozone effect is weak with warming (cooling) effect to the north (south) of $\sim 45^{\circ}$ N (Fig. 3c). The water vapor effect (Fig. 3e), which is dominated by the longwave (i.e. “greenhouse”) effect (matched well with the total column water vapor changes shown in Fig. 4a), provides significant warming (cooling) anomalies over northern India, Tibetan Plateau, and central Siberia (South China and western Siberia). Surface albedo provides overall strong negative contributions to the warming over the East Asian continent (Fig. 3f, –0.15 K), particularly over the Tibetan Plateau, Mongolia, and northern Siberia, which is directly linked to the changes in surface albedo (Fig. 4b). Besides, the surface albedo changes are concentrated over high-latitude (north of 60° N) and high-elevation regions (Tibetan Plateau and Mongolia) where snow/glacier changes are pronounced under global climate change (IPCC 2013). The cloud effect contributes

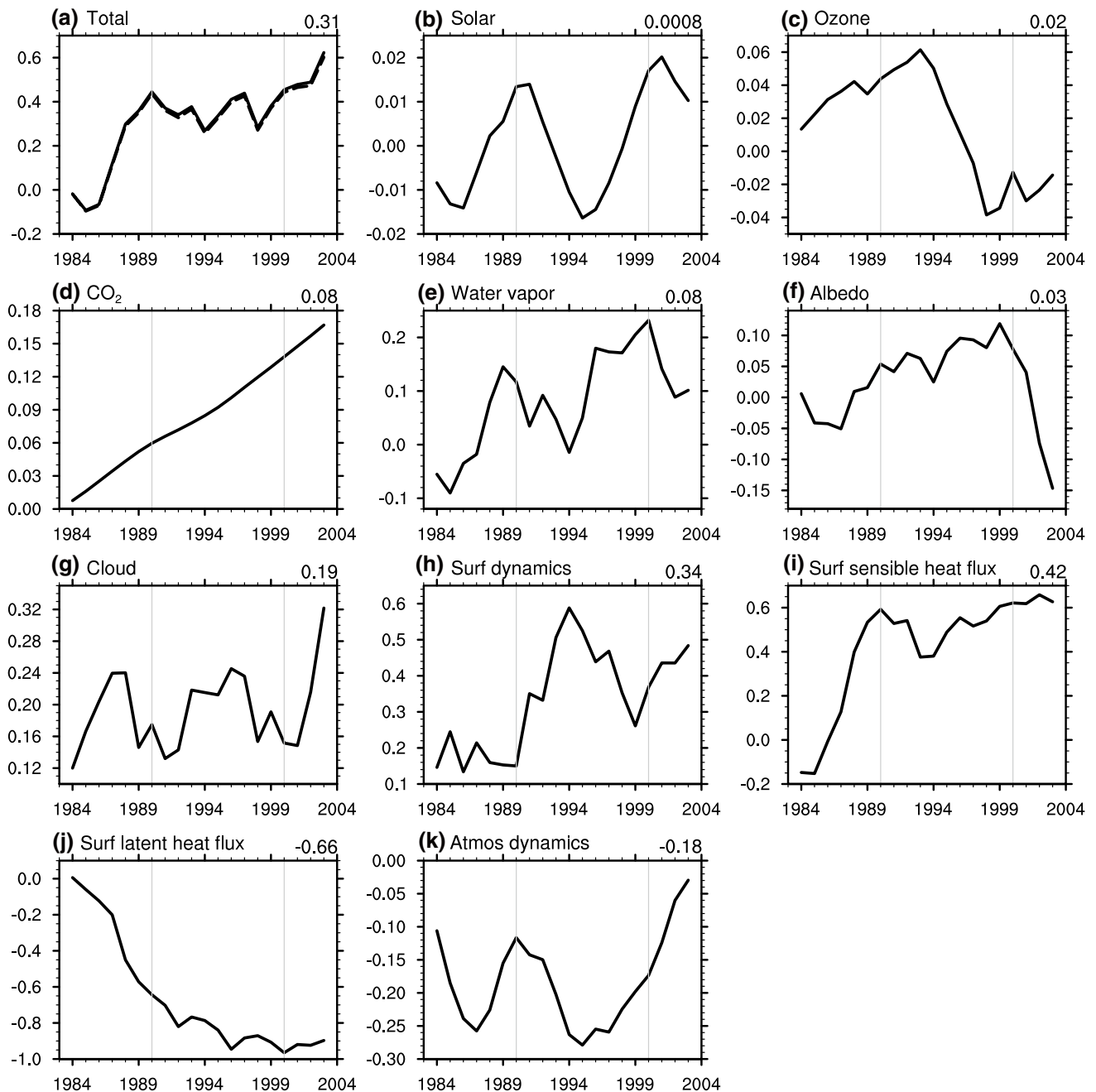


Fig. 1 Temporal evolutions of surface temperature (K) from 1984 to 2003 shown as the differences between the averages over individual 5-year segments and the average over the base state (1981–1985): the sum of partial temperature differences (K) derived from the CFRAM (solid line) and the ERA-Interim (dashed line) (a), and partial temperature differences (K) due to changes in solar irradiance (b), ozone

(c), CO₂ (d), water vapor (e), albedo (f), clouds (g), surface dynamics (h), surface sensible heat flux (i), surface latent heat flux (j), and atmospheric dynamics (k). The gray lines of each panel denote the year 1990 and 2000. The value on the upper right of each panel denotes the mean value of the corresponding solid curve

significantly to the warming over South China and southern Siberia, but reduces the warming over the Tibetan Plateau and India (Fig. 3g). Comparison of the partial temperature differences due to changes in clouds with the total cloud cover changes shown in Fig. 4c indicates that the cloud effect is dominated by the shortwave effect (decreasing cloud cover

induces more solar radiation reaching the surface and vice versa). This feature is consistent with results from previous studies where a significant decreasing trend in total cloud cover appears over China (Liu et al. 2004), particularly in eastern China (Xia 2010b). The increase of total cloud cover, shown in the ERA-Interim over western China (Fig. 4c), is

Fig. 2 **a** Surface albedo differences (%) and **b** snowfall differences (mm/day) between 2003 (2001–2005) and 1999 (1997–2001) from the ERA-Interim. The dots indicate values exceeding the 0.1 level of statistical significance according to the Student's t-test

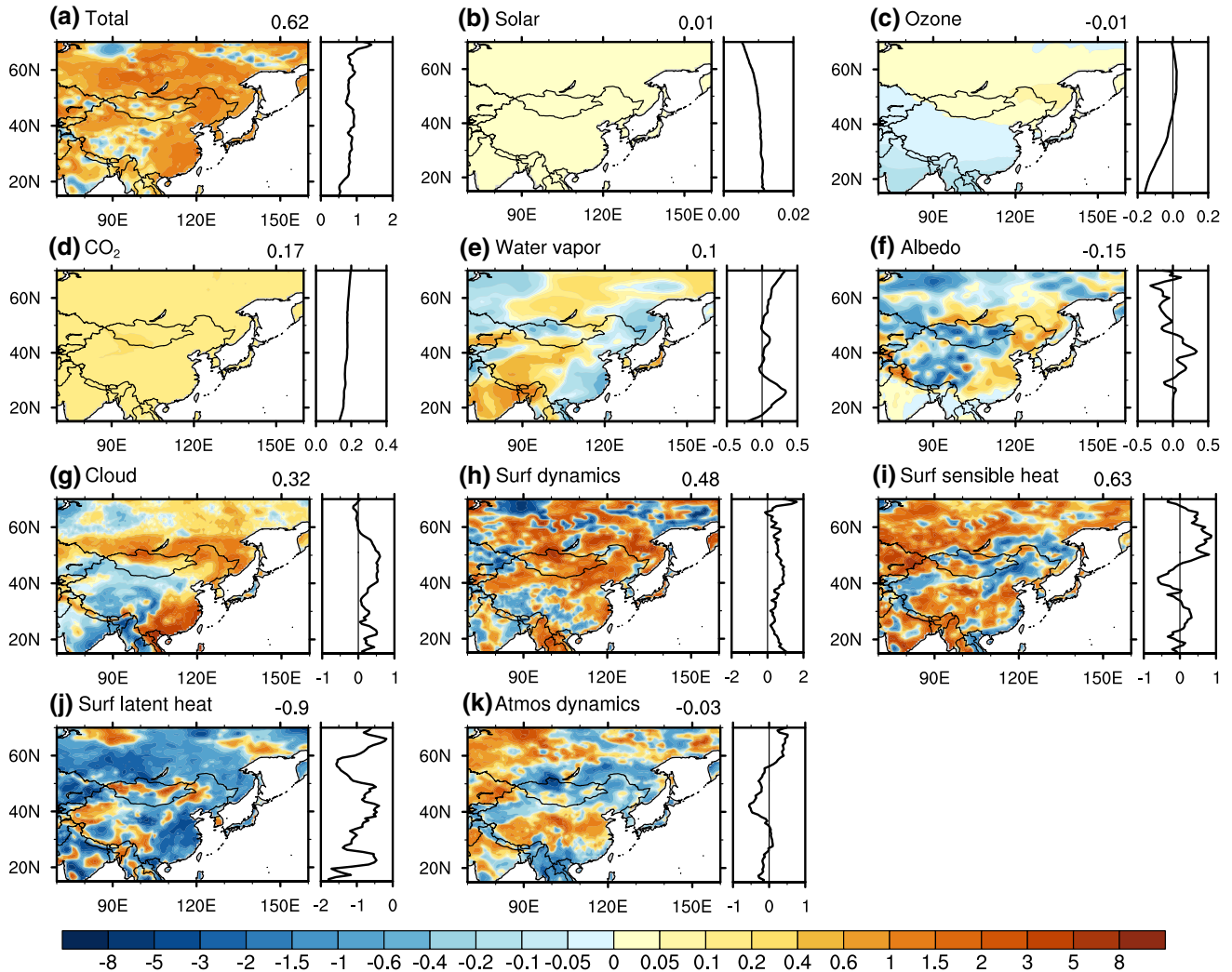
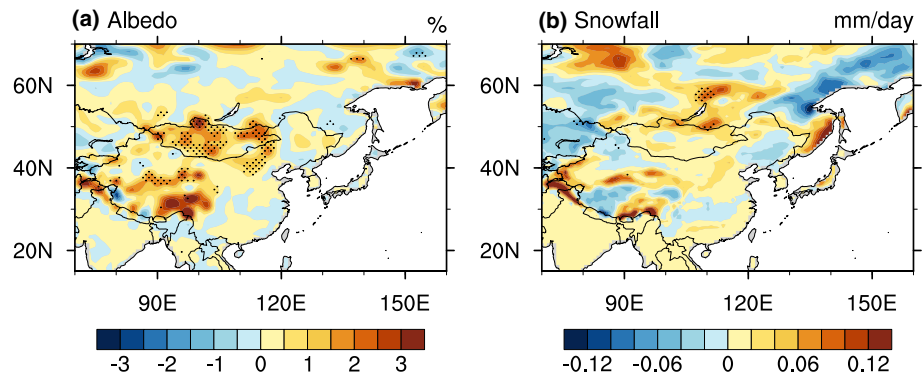


Fig. 3 Surface temperature differences (K) between 2003 (2001–2005) and base state (1981–1985): the sum of partial temperature differences (K) derived from the CFRAM (**a**), and partial temperature differences (K) due to changes in solar irradiance (**b**), ozone (**c**), CO_2 (**d**), water vapor (**e**), albedo (**f**), clouds (**g**), surface dynamics (**h**), sur-

face sensible heat flux (**i**), surface latent heat flux (**j**), and atmospheric dynamics (**k**). The value on the upper right of each panel denotes the area averaged value and the curve on the right of each panel denotes the meridional profile of zonally averaged values

likely due to the uncertainties of clouds in the ERA-Interim and lack of observations over the western China to constrain the reanalysis.

The surface dynamics plays a key role in the surface warming over the East Asian continent, particularly over southern Siberia, Mongolia, and northern China, with an

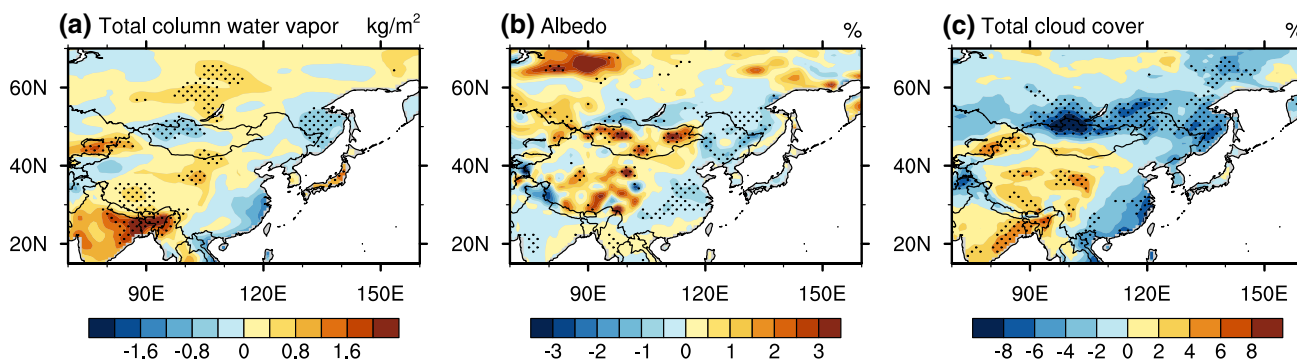


Fig. 4 **a** Total column water vapor differences (kg/m^2), **b** surface albedo differences (%), and **c** total cloud cover differences (%) between 2003 (2001–2005) and base state (1981–1985) from the

ERA-Interim. The dots indicate values exceeding the 0.1 level of statistical significance according to the Student's t-test

area averaged partial temperature differences of approximately 0.48 K (Fig. 3h). However, regional cooling effects of surface dynamics are documented over northern Siberia and Tibetan Plateau. These regional warming or cooling anomalies associated with surface dynamics are primarily related to the snow/ice melting/freezing over high-latitude (north of 40°N) and high-elevation regions, and soil heat diffusion over the low latitudes (south of 40°N). The sensible heat flux is a major contributor to the surface warming (Fig. 3i, 0.63 K), evidenced by excessive warming over Siberia, Tibetan Plateau, and central China. The latent heat flux acts as the main process to cool the surface through increased evaporation, particularly over Siberia and East China (Fig. 3j, -0.9 K). Although atmospheric dynamics provides overall weak negative contribution to the surface warming (Fig. 3k, -0.03 K), it tends to cool (warm) the surface where surface dynamics exhibits warming (cooling) effects, except over India and East China (Fig. 3k v.s. h).

3.2 Assessment of contributions by individual processes to decadal-scale surface temperature evolutions

In order to quantify the overall contribution of individual processes to the observed surface temperature evolution over the East Asian continent, we adopt the measure of “pattern-amplitude projection” (PAP) coefficient used in Park et al. (2012) and Deng et al. (2013). The PAP coefficient is defined as

$$PAP_i = \langle \Delta T \rangle \times \frac{\langle \Delta T_i \Delta T \rangle}{\langle (\Delta T)^2 \rangle}, \tag{4}$$

where ΔT and ΔT_i are the observed surface temperature differences with respect to the base state (1981–1985) and the partial surface temperature differences related to the i th process derived from the CFRAM, respectively. $\langle \rangle$ represents

the temporal average (for temporal PAP) or area average (for spatial PAP). The sum of all PAP_i equals to the temporal average or area average of the observed surface temperature differences for the temporal PAP or the spatial PAP, respectively.

First we obtain the temporal PAP coefficients for all processes utilizing the partial temperature results (corresponding to each 5-year segment) reported in Fig. 1. The temporal PAPs focus on the contribution of a process to the interannual-decadal fluctuations in the surface temperature evolution over East Asia, as well as the trend. The results are shown in Fig. 5a and the sum of PAPs converges to the area averaged temperature reported in Fig. 1a (0.31 K). The sensible heat flux is the main positive contributor to the surface temperature evolution over East Asia, followed by surface dynamics (mainly snow/ice freezing/melting, river runoff, and soil heat diffusion), clouds, water vapor, and CO_2 at a decreasing magnitude (Fig. 5a). Net negative contributions of latent heat flux and atmospheric dynamics to the surface temperature evolution is consistent with the previous discussions, since it tends to cool (warm) the surface through large-scale energy transport and convective/turbulent heat transport when surface gets warmer (cooler).

Next, we analyze the temporal evolutions of the spatial PAP coefficients calculated for an individual 5-year segment. For each segment, the sum of the PAPs converges to the total temperature differences (with respect to the 1981–1985 base state) area averaged over the East Asian continent (solid black curve in Fig. 5b). Here the spatial PAP emphasizes the contribution of a process to the spatial pattern of the observed surface temperature difference through pattern projection. Surface dynamics instead of sensible heat flux clearly dictates the spatial distribution of surface temperature evolution (Fig. 5b). The contribution of sensible heat flux has large interannual-decadal fluctuations, switching signs of contribution around early 1990s and early 2000s.

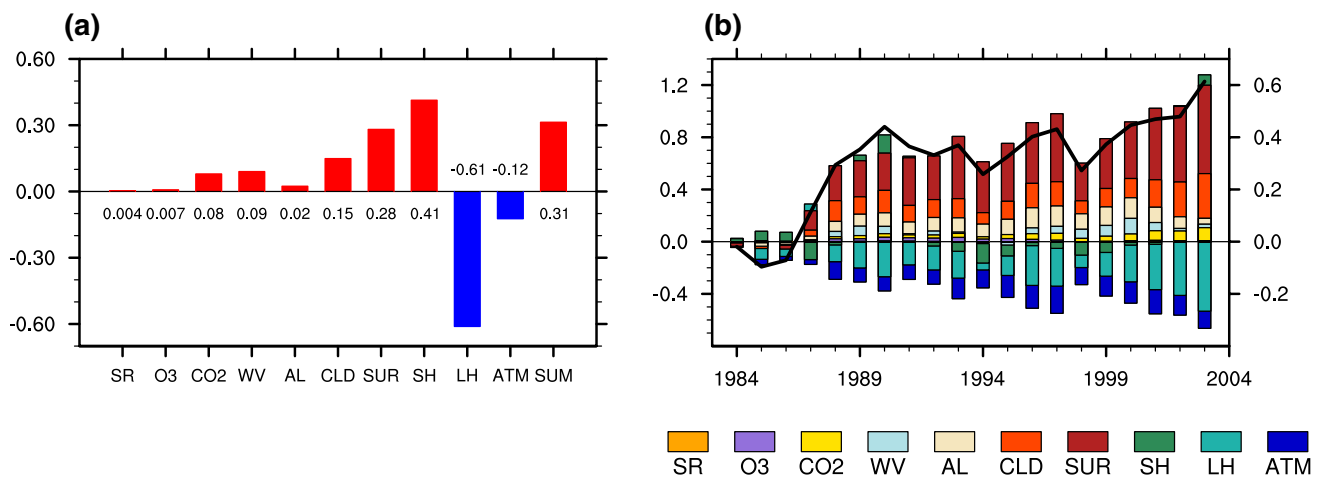


Fig. 5 **a** Temporal pattern-amplitude projection (PAP) coefficients (K) associated with the ten partial temperature differences shown in Fig. 1b–i and their sums. **b** Temporal evolution of the spatial PAP coefficients (K, refer to the left Y coordinate) associated with the same ten processes and their sums (solid black curves, refer to

the right Y coordinate). “SR”, “O3”, “CO2”, “WV”, “AL”, “CLD”, “SUR”, “SH”, “LH”, “ATM”, and “SUM” stand for solar irradiance, ozone, CO₂, water vapor, surface albedo, cloud, surface dynamics, surface sensible heat flux, surface latent heat flux, atmospheric dynamics, and the sum, respectively

The latent heat flux, together with atmospheric dynamics, tends to work against the warming, evidenced by the negative values through the whole period. In addition, the overall surface temperature evolution receives secondary positive contributions from processes due to the changes in clouds, albedo, water vapor, and CO₂. During the restored rapid warming after 1999, the contributions from the processes related to clouds and CO₂ changes become more important while the water vapor and albedo effects become smaller. However, it is hard to know whether the clouds effect is accurately represented due to the uncertainties in the ERA-Interim cloud fields as discussed previously.

3.3 Spatial structure of individual process contributions in the rapid warming and cooling periods

To further investigate the differences and similarities of contributions from individual processes to the extreme interannual temperature fluctuations over East Asia, we conduct additional two experiments using the CFRAM method. We define the rapid warming (cooling) period as the maximum increase (decrease) of surface temperature in two adjacent calendar years from 1981 to 2005 (without 5-year running average), which is the difference between 1988 and 1987 (0.80 K) for the rapid warming segment (between 1996 and 1995 (−0.94 K) for the rapid cooling segment). Then, we treat 1987 as the base state and 1988 as the warming climate state to contrast with the base state in the rapid warming experiment, while treating 1995 as the base state and 1996 as the cooling climate state to contrast with the base state in the rapid cooling experiment.

The rapid warming (cooling) surface temperature differences between 1988 and 1987 (1996 and 1995) are shown in Fig. 6a (Fig. 7a), and corresponding spatial distributions of the partial temperature differences associated with individual processes are displayed in Fig. 6b–k (Fig. 7b–k). The most pronounced feature is the excessive warming (cooling) over the high latitudes (north of 40°N) in the rapid warming (cooling) period (Figs. 6a, 7a). The growth of CO₂ concentration provides nearly uniform warming in both rapid warming and cooling periods with a value of 0.01 K (Figs. 6d, 7d). The partial temperature differences due to change in solar irradiance are weakly positive (negative) in the rapid warming (cooling) periods (Figs. 6b, 7b). The effect of ozone are reversed between the two periods (Figs. 6c, 7c), with strong cooling effect in the rapid cooling period (−0.22 K). The water vapor effect is stronger in the rapid warming period than that in the rapid cooling period (0.55 v.s. −0.18 K, Figs. 6e v.s. 7e), and plays a key role in the warming (cooling) anomalies occurred to the north 40°N in the rapid warming (cooling) period. Surface albedo has an overall significant positive (negative) effect on the warming (cooling), with great regional variations (Figs. 6f, 7f). Besides, the albedo effect could have large interannual fluctuations depending on the surface state, related to the snow cover, snow depth, snow density, and glacier melting. Although cloud changes provide nearly opposite contribution over East Asia between the two periods (Figs. 6g v.s. 7g, also see the meridional profile of zonal averaged partial temperature differences to the right), an overall negative effect is both found in the two periods. Surface dynamics is a major negative contributor to the surface warming or cooling in the rapid warming or cooling period, which is

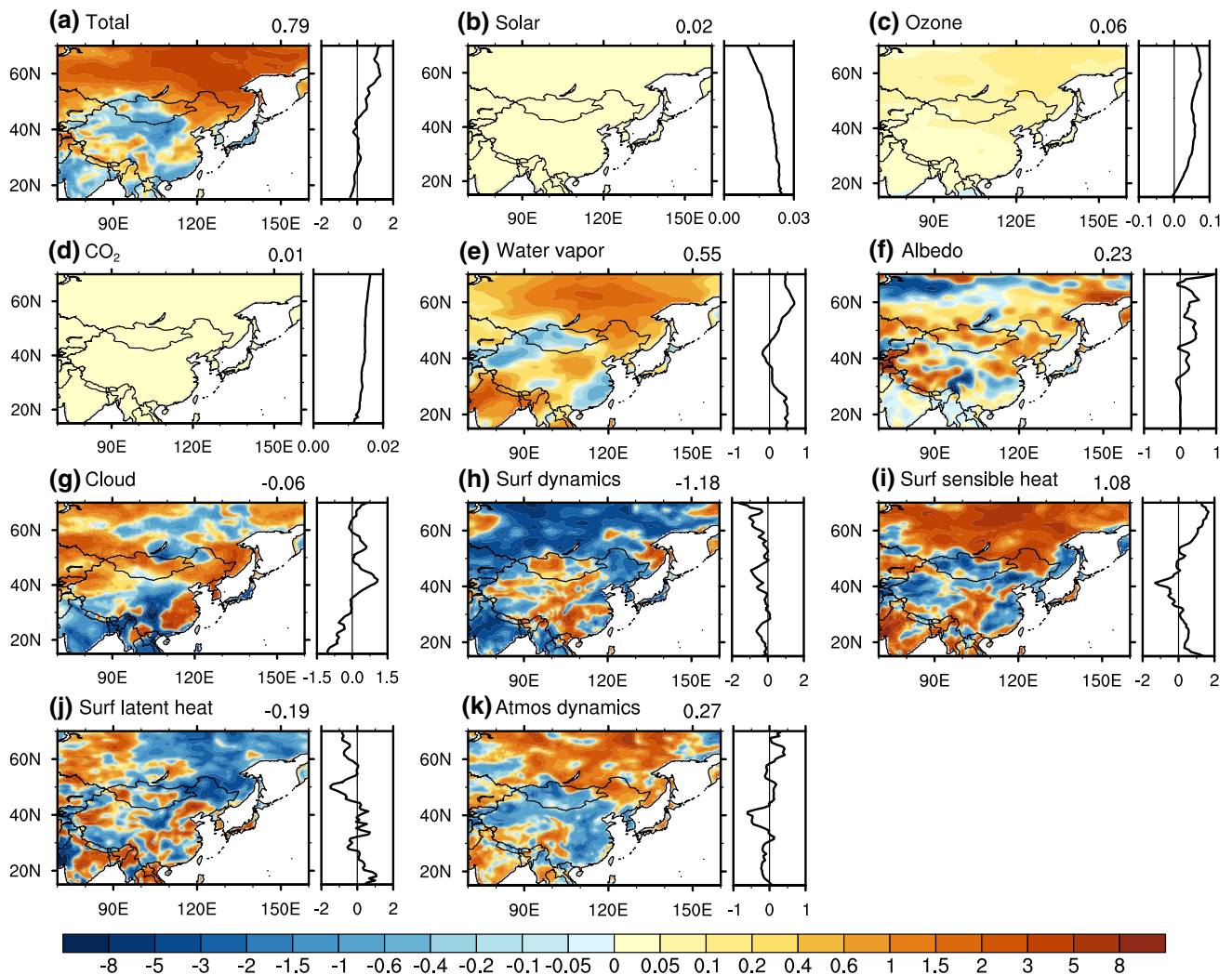


Fig. 6 Same as in Fig. 3, but for surface temperature difference (K) between 1988 and 1987

characterized by negative or positive partial temperature differences over a large portion of the high latitudes (north of 50°N , Figs. 6h, 7h). The latent heat flux, as an overall negative contributor to the warming or cooling (Figs. 6j, 7j), exhibits significant regional variations associated with changes in surface state-dependent evaporation (e.g., surface temperature, soil moisture, and soil temperature). While the sensible heat flux plays a critical role in providing positive contributions to the warming or cooling over the high latitudes in the rapid warming or cooling period (Figs. 6i, 7i). Cloud effects tend to compensate those of the sensible heat flux in the low latitudes (south of 40°N) (Fig. 6i v.s. Figs. 6g, 7i v.s. Fig. 7g). The atmospheric dynamics acts as a secondary positive contributor to the warming or cooling, documented by positive (negative) contribution over the high latitudes (East China). The behaviors of surface dynamics and atmospheric dynamics are reversed compared to those in the decadal surface temperature changes discussed in Sect. 3.1

and 3.2, suggesting that interannual surface temperature fluctuations are closely tied to the large-scale atmospheric circulation changes (e.g., changes in the frequency of cold air outbreaks and phase of the Arctic Oscillation). Note that the behavior of surface dynamics might be case dependent due to the influences of interannual large-scale atmospheric circulation fluctuations and errors associated with the use of offline radiative transfer calculations and linearization of radiative energy perturbations as discussed previously.

To further quantify and compare the overall contributions of individual processes to the magnitude and spatial distribution of surface temperature differences in the rapid warming and cooling periods, beyond the surface temperature differences shown in Figs. 6 and 7, we calculate the spatial PAP to the observed temperature anomalies over East Asia. As displayed in Fig. 8a, the rapid warming pattern receives major positive contribution from sensible heat flux with atmospheric dynamics, water vapor, clouds, and albedo

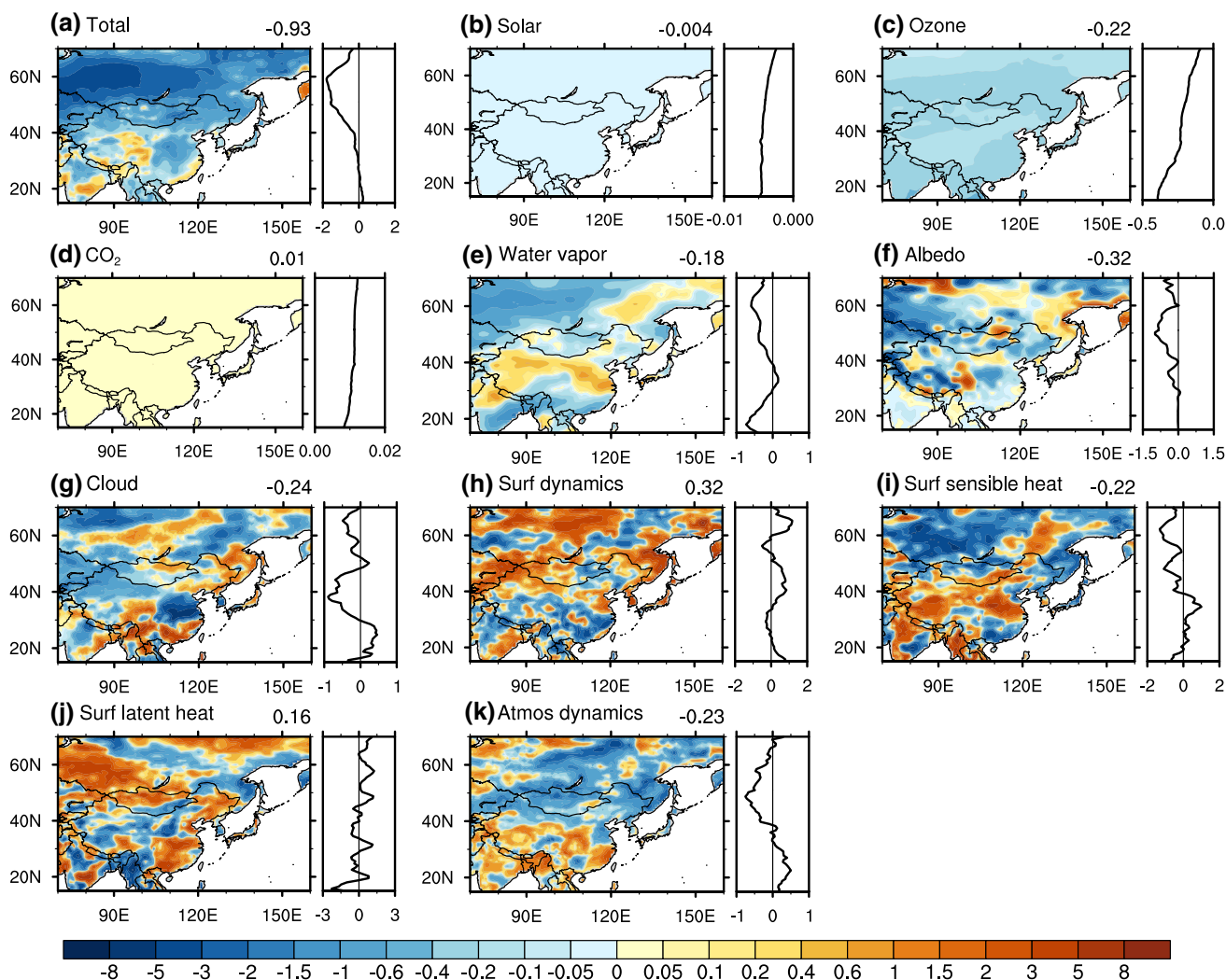


Fig. 7 Same as in Fig. 6, but for surface temperature difference (K) between 1996 and 1995

changes providing secondary contributions. A major negative contribution from surface dynamics tends to cool the surface as discussed previously. The latent heat flux gives secondary negative contribution to the rapid warming. In the rapid cooling period, the signs of the major contributions from physical and dynamical processes are nearly opposite to those seen in the rapid warming period (Fig. 8b v.s. a). The magnitudes of contributions from surface dynamics and sensible heat flux are much smaller in the rapid cooling period than those in the rapid warming period. In addition, the importance of processes related to solar irradiance, ozone, and CO_2 , are to a less degree compared to other processes. These results show that the processes contributing to rapid warming tend to work in reversed orders as in the rapid cooling case. The similarity of the relative contributions of individual processes in the rapid warming (cooling) period suggests that the rapid warming (cooling) discussed here share some common physical origins.

4 Concluding remarks

In this study, we have partitioned the temporal evolutions of the surface temperature over the East Asian continent from 1981 to 2005 into components associated with individual radiative and non-radiative (dynamical) processes in the context of the CFRAM method utilizing the ERA-Interim reanalysis. A process-based decomposition of surface temperature differences between two decades (early 2000s and early 1980s) is investigated. We identify two periods of rapid warming occurring in the late 1980s and the early 2000s, with a transient pause of warming between them. The strongest warming is found over southern Siberia and East China. The rising CO_2 concentration provides sustained positive contributions to the warming trend, while the contributions from other processes have large interannual-decadal fluctuations. Sensible heat flux and surface dynamics (mainly snow/ice freezing/melting, river runoff, and soil heat diffusion)

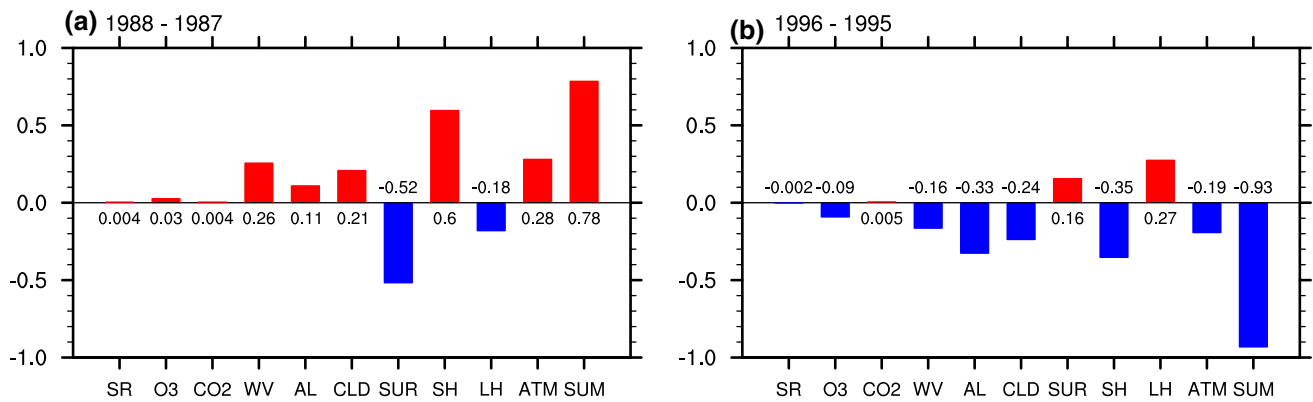


Fig. 8 Spatial pattern-amplitude projection (PAP) coefficients associated with the ten surface partial temperature anomalies (K): **a** the difference (K) between 1988 and 1987; **b** the difference (K) between 1996 and 1995. “SR”, “O3”, “CO2”, “WV”, “AL”, “CLD”, “SUR”,

“SH”, “LH”, “ATM”, and “SUM” stand for solar irradiance, ozone, CO₂, water vapor, surface albedo, cloud, surface dynamics, surface sensible heat flux, surface latent heat flux, atmospheric dynamics, and the sum of ten PAP coefficients, respectively

are the most critical processes dictating the surface temperature evolution, with latent heat flux and atmospheric dynamics working against them through large-scale energy transport and convective/turbulent heat transport. However, surface dynamics provides major contribution to the spatial distribution of surface temperature anomalies through the entire period, while the contribution of sensible heat flux has large interannual-decadal fluctuations with sign switch. Cloud via its shortwave effects act as the secondary positive contributor to the surface temperature evolution, particularly over southern Siberia and South China. Water vapor effect contributes significant warming (cooling) anomalies over northern India, Tibetan Plateau, and central Siberia (South China and western Siberia), and is dominated by the longwave (i.e., “greenhouse”) effect. The effect of surface albedo is important for regional warming/cooling over high-latitude and at high-elevation regions, where snow cover and glacier melting are significant under global climate change. The weakened albedo effect in early 2000s was related to the increase in snowfall over Siberia, Mongolia, and the Tibetan Plateau. Finally, the impacts of solar irradiance and ozone change are relatively small.

An examination of the contributions by individual processes in the interannual rapid warming (1988 v.s. 1987) and cooling (1996 v.s. 1995) periods shows that the signs of the contributions from those physical processes are almost opposite between the two periods, suggesting that the rapid warming and cooling discussed here share some common physical origins. The strongest warming or cooling is observed over the high latitudes (north of 40°N). The rapid warming pattern receives major positive contributions from sensible heat flux, with changes in atmospheric dynamics, water vapor, clouds, and albedo providing secondary

contributions, while surface dynamics and latent heat flux providing negative contribution. The behaviors of surface dynamics and atmospheric dynamics are reversed compared to those in the decadal surface temperature changes, suggesting that interannual surface temperature fluctuations are closely tied to the large-scale atmospheric circulation changes. Although the processes contributing to rapid warming tend to work in reversed orders as in rapid cooling period, the magnitudes of contributions from surface dynamics and sensible heat flux are much smaller in the rapid cooling period than those in the rapid warming period.

Note that the results about partitioning surface temperature reported here are based on the principle of energy balance in an atmosphere-surface column through the CFRAM method. In this sense, the CFRAM analysis represents essentially an examination of the partitioning of local energy perturbations in the climate system and does not provide explicitly any information regarding the causality of the processes. In other words, the CFRAM does not suggest what processes initiate the changes in temperature and what processes follow. However, it is an efficient off-line diagnostic tool to decompose temperature difference into addable, process-based partial temperature differences, which can be utilized to assess the relative contributions of them. We will use additional observational data (e.g. the NASA MERRA-2 reanalysis) to further verify the conclusions drawn here, particularly the cloud effects.

Acknowledgements The ERA-Interim dataset was provided by the European Centre for Medium-range Weather Forecasts. The Global Precipitation Climatology Project combined precipitation dataset was provided by the US National Oceanic and Atmospheric Administration. Lin and Yang are supported by the National Key Scientific Research Plan of China (Grant 2014CB953904), the National Natural Science

Foundation of China (Grants 91637208, 41690123, and 41690120), and the “111-Plan” Project of China (Grant B17049). Chen and Deng are supported by the National Science Foundation (Grants AGS-1147601, AGS-1354402, and AGS-1445956).

References

- Bao X, Zhang F (2013) Evaluation of NCEP–CFSR, NCEP–NCAR, ERA-Interim, and ERA-40 reanalysis datasets against independent sounding observations over the Tibetan Plateau. *J Clim* 26:206–214
- Cai M, Lu J (2009) A new framework for isolating individual feedback processes in coupled general circulation climate models. Part II: method demonstrations and comparisons. *Clim Dyn* 32:887–900
- Chen J-P, Chen I-J, Tsai I-C (2016) Dynamic feedback of aerosol effects on the East Asian summer monsoon. *J Clim* 29:6137–6149
- Chen J, Deng Y, Lin W, Yang S (2017) A process-based assessment of decadal-scale surface temperature evolutions in the NCAR CCSM4’s 25-year hindcast experiments. *J Clim*. doi:10.1175/JCLI-D-16-0869.1
- Chung CE, Ramanathan V, Carmichael G, Kulkarni S, Tang Y, Adhikary B, Leung LR, Qian Y (2010) Anthropogenic aerosol radiative forcing in Asia derived from regional models with atmospheric and aerosol data assimilation. *Atmos Chem Phys* 10:6007–6024
- Dee DP, Uppala SM, Simmons AJ, Berrisford P, Poli P, Kobayashi S, Andrae U, Balmaseda MA, Balsamo G, Bauer P, Bechtold P, Beljaars ACM, van de Berg L, Bidlot J, Bormann N, Delsol C, Dragani R, Fuentes M, Geer AJ, Haimberger L, Healy SB, Hersbach H, Hólm EV, Isaksen I, Kållberg P, Köhler M, Matricardi M, McNally AP, Monge-Sanz BM, Morcrette JJ, Park BK, Peubey C, de Rosnay P, Tavolato C, Thépaut JN, Vitart F (2011) The ERA-Interim reanalysis: configuration and performance of the data assimilation system. *Q J R Meteor Soc* 137:553–597
- Deng Y, Park T-W, Cai M (2012) Process-based decomposition of the global surface temperature response to El Niño in boreal winter. *J Atmos Sci* 69:1706–1712
- Deng Y, Park T-W, Cai M (2013) Radiative and dynamical forcing of the surface and atmospheric temperature anomalies associated with the northern annular mode. *J Clim* 26:5124–5138
- Duan A, Xiao Z (2015) Does the climate warming hiatus exist over the Tibetan Plateau? *Sci Rep* 5:13711
- Feng J-M, Wang Y-L, Ma Z-G, Liu Y-H (2012) Simulating the regional impacts of urbanization and anthropogenic heat release on climate across China. *J Clim* 25:7187–7203
- Fu Q, Liou KN (1992) On the correlated k-distribution method for radiative transfer in nonhomogeneous atmospheres. *J Atmos Sci* 49:2139–2156
- Fu Q, Liou KN (1993) Parameterization of the radiative properties of cirrus clouds. *J Atmos Sci* 50:2008–2025
- Hu ZZ, Yang S, Wu R (2003) Long-term climate variations in China and global warming signals. *J Geophys Res*. doi:10.1029/2003JD003651
- Hu Z, Zhang C, Hu Q, Tian H (2014) Temperature changes in central Asia from 1979 to 2011 based on multiple datasets. *J Clim* 27:1143–1167
- Hu X, Yang S, Cai M (2016) Contrasting the eastern Pacific El Niño and the central Pacific El Niño: process-based feedback attribution. *Clim Dyn* 47:2413–2424
- Hu X, Li Y, Yang S, Deng Y, Cai M (2017) Process-based decomposition of the decadal climate difference between 2002–13 and 1984–95. *J Clim* 30:4373–4393
- IPCC (2013) Climate change 2013: the physical science basis. In: Stocker TF, Qin D, Plattner GK et al (eds) Contribution of working group I to the fifth assessment report of the intergovernmental panel on climate change. Cambridge University Press, Cambridge
- Jeong J-H, Ou T, Linderholm HW, Kim B-M, Kim S-J, Kug J-S, Chen D (2011) Recent recovery of the Siberian high intensity. *J Geophys Res Atmos* 116:D23102. doi:10.1029/2011JD015904
- Kaufman YJ, Tanre D, Boucher O (2002) A satellite view of aerosols in the climate system. *Nature* 419:215–223
- Li Z, Li C, Chen H, Tsay SC, Holben B, Huang J, Li B, Maring H, Qian Y, Shi G, Xia X, Yin Y, Zheng Y, Zhuang G (2011) East Asian studies of tropospheric aerosols and their impact on regional climate (EAST-AIRC): an overview. *J Geophys Res Atmos* 116:D00K34. doi:10.1029/2010JD015257
- Li Z, Lau WKM, Ramanathan V, Wu G, Ding Y, Manoj MG, Liu J, Qian Y, Li J, Zhou T, Fan J, Rosenfeld D, Ming Y, Wang Y, Huang J, Wang B, Xu X, Lee SS, Cribb M, Zhang F, Yang X, Takemura T, Wang K, Xia X, Yin Y, Zhang H, Guo J, Zhai PM, Sugimoto N, Babu SS, Brasseur GP (2016) Aerosol and monsoon climate interactions over Asia. *Rev Geophys* 54. doi:10.1002/2015RG000500
- Liu B, Zhou T (2017) Atmospheric footprint of the recent warming slowdown. *Sci Rep* 7:40947
- Liu B, Xu M, Henderson M, Qi Y, Li Y (2004) Taking China’s temperature: daily range, warming trends, and regional variations, 1955–2000. *J Clim* 17:4453–4462
- Liu B, Zhou T, Lu J (2015) Quantifying contributions of model processes to the surface temperature bias in FGOALS-g2. *J Adv Model Earth Syst* 7:1519–1533
- Lu J, Cai M (2009) A new framework for isolating individual feedback processes in coupled general circulation climate models. Part I: formulation. *Clim Dyn* 32:873–885
- Meehl GA, Teng H (2012) Case studies for initialized decadal hindcasts and predictions for the Pacific region. *Geophys Res Lett* 39:L22705. doi:10.1029/2012GL053423
- Park H-S, Sohn BJ (2010) Recent trends in changes of vegetation over East Asia coupled with temperature and rainfall variations. *J Geophys Res Atmos* 115:D14101. doi:10.1029/2009JD012752
- Park T-W, Deng Y, Cai M (2012) Feedback attribution of the El Niño–southern oscillation–related atmospheric and surface temperature anomalies. *J Geophys Res Atmos* 117:D23101. doi:10.1029/2012JD018468
- Park T-W, Deng Y, Cai M, Jeong J-H, Zhou R (2013) A dissection of the surface temperature biases in the community earth system model. *Clim Dyn* 43:2043–2059
- Ramanathan V, Carmichael G (2008) Global and regional climate changes due to black carbon. *Nat Geosci* 1:221–227
- Ren G, Zhou Y, Chu Z, Zhou J, Zhang A, Guo J, Liu X (2008) Urbanization effects on observed surface air temperature trends in North China. *J Clim* 21:1333–1348
- Ren R, Sun S, Yang Y, Li Q (2016) Summer SST anomalies in the Indian Ocean and the seasonal timing of ENSO decay phase. *Clim Dyn* 47:1827–1844
- Romanovsky VE, Drozdov DS, Oberman NG, Malkova GV, Kholodov AL, Marchenko SS, Moskalenko NG, Sergeev DO, Ukrainseva NG, Abramov AA, Gilichinsky DA, Vasiliev AA (2010) Thermal state of permafrost in Russia. *Permafrost Periglacial Process* 21:136–155
- Rosenfeld D, Andreae MO, Asmi A, Chin M, de Leeuw G, Donovan DP, Kahn R, Kinne S, Kivekäs N, Kulmala M, Lau W, Schmidt KS, Suni T, Wagner T, Wild M, Quaas J (2014) Global observations of aerosol–cloud–precipitation–climate interactions. *Rev Geophys* 52:750–808
- Saha S, Moorthi S, Wu X, Wang J, Nadiga S, Tripp P, Behringer D, Hou Y-T, Chuang H-y, Iredell M, Ek M, Meng J, Yang R, Mendez MP, Dool Hvd, Zhang Q, Wang W, Chen M, Becker E (2014) The NCEP Climate Forecast System version 2. *J Clim* 27:2185–2208
- Seinfeld JH, Carmichael GR, Arimoto R, Conant WC, Brechtel FJ, Bates TS, Cahill TA, Clarke AD, Doherty SJ, Flatau PJ, Huebert

- BJ, Kim J, Markowicz KM, Quinn PK, Russell LM, Russell PB, Shimizu A, Shinozuka Y, Song CH, Tang Y, Uno I, Vogelmann AM, Weber RJ, Woo J-H, Zhang XY (2004) ACE-ASIA: regional climatic and atmospheric chemical effects of Asian dust and pollution. *Bull Am Meteorol Soc* 85:367–380
- Serreze MC, Walsh JE, Chapin FS, Osterkamp T, Dyurgerov M, Romanovsky V, Oechel WC, Morison J, Zhang T, Barry RG (2000) Observational evidence of recent change in the northern high-latitude environment. *Clim Chang* 46:159–207
- Sun Y, Zhang X, Ren G, Zwiers FW, Hu T (2016) Contribution of urbanization to warming in China. *Nat Clim Chang* 6:706–709
- Taylor KE, Stouffer RJ, Meehl GA (2012) An overview of CMIP5 and the experiment design. *Bull Am Meteorol Soc* 93:485–498
- Wang JXL, Gaffen DJ (2001) Late-twentieth-century climatology and trends of surface humidity and temperature in China. *J Clim* 14:2833–2845
- Wang A, Zeng X (2012) Evaluation of multireanalysis products with in situ observations over the Tibetan Plateau. *J Geophys Res Atmos* 117:D05102. doi:10.1029/2011JD016553
- Wang J, Yan Z, Jones PD, Xia J (2013) On “observation minus reanalysis” method: a view from multidecadal variability. *J Geophys Res Atmos* 118:7450–7458
- Xia X (2010a) A closer looking at dimming and brightening in China during 1961–2005. *Ann Geophys* 28:1121–1132
- Xia X (2010b) Spatiotemporal changes in sunshine duration and cloud amount as well as their relationship in China during 1954–2005. *J Geophys Res Atmos* 115:D00K06. doi:10.1029/2009JD012879
- Yang Y, Ren R (2017) On the contrasting decadal changes of diurnal surface temperature range between the Tibetan Plateau and southeastern China during the 1980s–2000s. *Adv Atmos Sci* 34:181–198
- Yang D, Kane DL, Hinzman LD, Zhang X, Zhang T, Ye H (2002) Siberian Lena River hydrologic regime and recent change. *J Geophys Res Atmos* 107(D23):4694. doi:10.1029/2002JD002542
- Yang X, Hou Y, Chen B (2011) Observed surface warming induced by urbanization in east China. *J Geophys Res Atmos* 116:D14113. doi:10.1029/2010JD015452
- Yang Y, Ren R, Cai M, Rao J (2015) Attributing analysis on the model bias in surface temperature in the climate system model FGOALS-s2 through a process-based decomposition method. *Adv Atmos Sci* 32:457–469
- Ye K, Wu R, Liu Y (2015) Interdecadal change of Eurasian snow, surface temperature, and atmospheric circulation in the late 1980s. *J Geophys Res Atmos* 120:2738–2753